J Therm Anal Calorim (2010) 99:179–189
DOI 10.1007/s10973-009-0149-6

Thermal behavior and phase transformations of nanosized carbonate apatite (Syria)

V. Petkova · V. Yaneva

Received: 19 December 2008 / Accepted: 7 April 2009 / Published online: 19 June 2009

Abstract The phase transformations of Syrian phosphorite upon mechanochemical activation are examined in the present work. The latter is carried out in planetary mill equipped with 20 mm steel milling bodies and duration from 30 to 300 min. The established by means of DTA, DTG, TG analyses transformation of non-activated carbonate fluorine apatite type B into the carbonate hydroxyl fluorine apatite (COHFAp) mixed type A2-B leads to substantial changes in the properties of the activated samples expressed in lowering the degree of crystallinity, strong defectiveness of the structure, and increase of the citric solubility. The thermal analysis gives evidence for the decomposition of the carbonate-containing component within the phosphorite, as from the positions placed in the vicinity of the hexagonal 6_3 axis (type A2), as well as from the positions of the phosphate ion (type B), and from the free carbonates. The data from the thermal analysis, the powder X-ray analysis and the infrared spectroscopy give also evidence for phase transformations of the activated apatite (with admixtures of quartz and calcite) into $Ca_{10}FOH(PO_4)_6$, β-$Ca_3(PO_4)_2$, $Ca_4P_2O_9$, $Ca_3(PO_4)_2 \cdot Ca_2SiO_4$ and for that one of the quartz—into larnite and wollastonite. The influence of the α-quartz as a concomitant mineral is considered to be positive. The α-quartz forms Si–O–Si–OH bonds retaining humidity in the solid phase thus facilitating the isomorphous substitution $OH^- \rightarrow F^-$ with the subsequent formation of partially substituted COHFAp. Calcium silicophosphate and $Ca_4P_2O_9$ are obtained upon its further heating. The presented here results settle a perspective route for processing of low-grade phosphate raw materials by means of tribothermal treatment aiming at preparation of condensed phosphates suitable for application as slowly acting fertilizer components.

Keywords Carbonate-Apatite · Infrared spectroscopy · Nanosize material · Thermal analysis · X-ray diffraction

V. Petkova (✉)
Bulgarian Academy of Sciences, Central Laboratory of Mineralogy and Crystallography, "Academic G. Bonchev" Str. bl.107, 1113 Sofia, Bulgaria
e-mail: vilmapetkova@gmail.com

V. Yaneva
Technical University of Varna, 1 Studentska Str, 9010 Varna, Bulgaria

Introduction

The exhaustion of the high-grade phosphorous deposits as well as the ecological problems arising from the traditional technologies for preparation of phosphorous fertilizers and inorganic acids pose the problem for finding smart and rational solutions for application of new methods for processing of inefficient phosphate raw materials. These are generally ore deposits of relatively low content of useful components and high content of concomitant minerals such as carbonates, silicates, etc. Thus, the mechanochemical activation as a route for treatment of phosphate raw materials of sedimentary origin characterized by low $P_2O_5^{total}$ content and high admixture content turns out to be a perspective initiative [1–3]. The combination of thermal and spectroscopic methods provides the opportunity to follow the phase transformations occurring upon mechanochemical [1] and thermal treatment of various apatite isomorphous

modifications as well as those ones of the concomitant minerals [2–11]. The products of the thermal decomposition of these multiphase samples as well as the impact of the concomitant minerals such as calcite and quartz over the phase formation are of interest. Subject of the present investigation are samples of Syrian phosphorite.

In our previous study [12] it was found that upon mechanochemical activation of apatite from Syria a nanosized phase is formed which properties substantially differ from those ones of its traditional chemical analogs. The spectroscopic investigations have given evidence for substantial structural changes of the nanosized products being due to the incorporation of CO_2 and OH^- in the apatite structure.

The present article aims at further clarification of the results from the mechanochemical activation of nanosized apatite from Syria by means of thermal, spectroscopic methods, and powder X-ray analysis. Special attention is paid to the phase transformations.

Analytical procedures

Subject of the study is Syrian phosphorite characterized by the following chemical composition: 29.5% $P_2O_5^{total}$; 6.9% $P_2O_5^{ass}$ (in 2% citric acid); 3.2% F; 46.5% CaO; 0.55% R_2O_3 (R = Al, Fe); 1.1% SO_3; 7.3% SiO_2; 0.35% MgO; 0.05% Cl; 6.2% CO_2; moisture content 3.14% and average granulometric particle size of 0.08 mm.

The mechanochemical activation (MA) was carried out in a planetary mill Pulverisette-5, Fritsch Co (Germany) at a rotating speed of 320 min^{-1}, activation time from 30 to 300 min, type of milling bodies—plain steel, weight of the bodies of 510 g, diameter of the milling bodies of 20 mm, sample weight 20 g.

Thermogravimetric and differential thermal analyses (TG-DTG-DTA) were performed on a Stanton Redcroft thermal analyzer STA 780 (England) in the temperature range 293–1,400 K, with a heating rate of 10 K min^{-1}, sample weight of $10.0 \pm 0.2.10^{-3}$ g. Zirconium melting pots of d = 4.5 mm were used and the purging gas was 100% clear, dry air and flow-rate 50 mL min^{-1}.

The powder X-ray diffraction (XRD) measurements of the samples were performed on a DRON 3 M diffractometer with a horizontal Bragg-Brentano goniometer (radius of 192 mm) using a Fe-filtered Co-K_α radiation (40 kV, 28 mA). A step-scan technique was applied with a step size of 0.02 $^o2\theta$ and 3 s per step in the range 8–60 $^o2\theta$.

The diffractometer was externally calibrated with quartz and Si standards. Before the XRD experiments the samples were ground in agate mortar and the front-loaded pressed powder specimens were measured at room temperature.

Phase identification was performed using the index-file PDF (Powder Diffraction File, ICDD, 2001).

The Fourier transform infrared (FTIR) spectra were taken on a Bruker Tensor 37 spectrometer, using KBr pellet technique. A resolution of 2 cm^{-1} was used collecting 120 scans for each sample.

Results and discussion

The powder XRD and IR data have given evidence that in the course of the activation an active phase has been formed consisting of apatite, transformed to various extents and some new phases with close or overlapping diffraction lines and vibration bands [12]. The same study has established that the non-activated Syrian phosphorite used as starting material is in fact fluorine apatite with a partial substitution of the phosphate ions by carbonate ones which defines it as carbonate fluorine apatite (CFAp), type B. The formation of hydrogen bonds (–F···HO–) has been detected in the apatite structure of samples activated for 30–300 min and their presence has been considered as being due to partial substitution of F^- by OH^-, taking place in the course of activation [1, 3, 13, 14]. Incorporation of the hydroxyl group in the apatite structure facilitates its local destruction along the (211), (202), (300) planes of dissolution. The spectroscopic studies have given evidence that the carbonate ion takes part in the substitution as in the positions of the phosphate ion as well as in the positions of F^- along the 6_3 axis in the apatite structure. According to the powder XRD data, the formation of new phases has taken place such as: $Ca_{10}FOH(PO_4)_6$ (OHFAp) and $Ca_{10}(PO_4)_6CO_3$ (CAp), and the formation of $Ca_{10}(PO_4)_5CO_3OHF$ (COHFAp) has not been excluded. The IR spectroscopic data has established relocation of the carbonate ion in the interval 1,400–1,550 cm^{-1} (v_3) from the tetrahedral positions (B type) in the vacancies of Ca^{2+} in the vicinity of the hexagonal 6_3 axis (A2 type substitution), which is in accordance with the results of numerous investigators [15–21]. The established phase and isomorphous transformations in the activated samples give evidence that the mechanical activation has a "micro-level" impact, expressed in change of the chemical bond strength and additional deformations in the polyhedra. Simultaneously, substantially smaller in size crystallites are formed with altered lattice parameters and increased degree of structural defects.

The obtained by the mechanochemical activation product presents metastable and of elevated dispersion natural apatite, characterized by increased content of $P_2O_5^{ass}$ which is close by its chemical properties to the citrically soluble phosphorous fertilizers.

The $P_2O_5^{ass}$ solubility in 2% citric acid increases from 24.6% for non-activated apatite to 54.5% for activated for 300 min sample and in ammonium citrate—from 13.1 to 60.1%. The particle sizes of mechanochemicaly activated samples decrease to nano-scales along certain crystallographic planes—from 43.2 nm (non-activated apatite) to 9–12 nm (activated for 300 min sample) [12].

Having in mind the complex composition of the initial phosphorite, one should anticipate numerous consecutive and secondary chemical interactions in the course of the activation with the predominant participation of $Ca_5F(PO_4)_3$ in them. Thermal treatment of the activated samples up to 1,372 K in air has been performed in order to characterize in details the structural changes in $Ca_5F(PO_4)_3$ and to examine the phase transformations attending the mechanochemical activation. The thermally treated run-products are investigated by means of powder X-ray diffraction and infrared spectroscopy.

Powder XRD phase analysis

Powder XRD patterns of solid products from the thermal decomposition of the activated nano-sized samples are presented in Fig. 1a–d and Table 1. The solid phases obtained after the mechanochemical activation of the samples, identified and commented in details in [12] are presented for clarity in Table 1.

These data reveal partial transformation of: CFAp type B (non-activated Syrian phosphorite, sample A) [12] into whitlockite—β-$Ca_3(PO_4)_2$ (β-C_3P); α-quartz into γ-larnite—γ-Ca_2SiO_4 (γ-C_2Si) and wollastonite—$CaSiO_3$ (CSi). Among the nanosized activated samples COHFAp [12] transforms into β-C_3P and $Ca_4P_2O_9$ (TTCP), as well as in $Ca_3(PO_4)_2 \cdot Ca_2SiO_4$ (CSiP). The reflection lines of α-quartz disappear as it takes part in the thermal reactions bringing to its depletion as a separate phase. As in the case of the non-activated apatite, SiO_2 takes part in high-

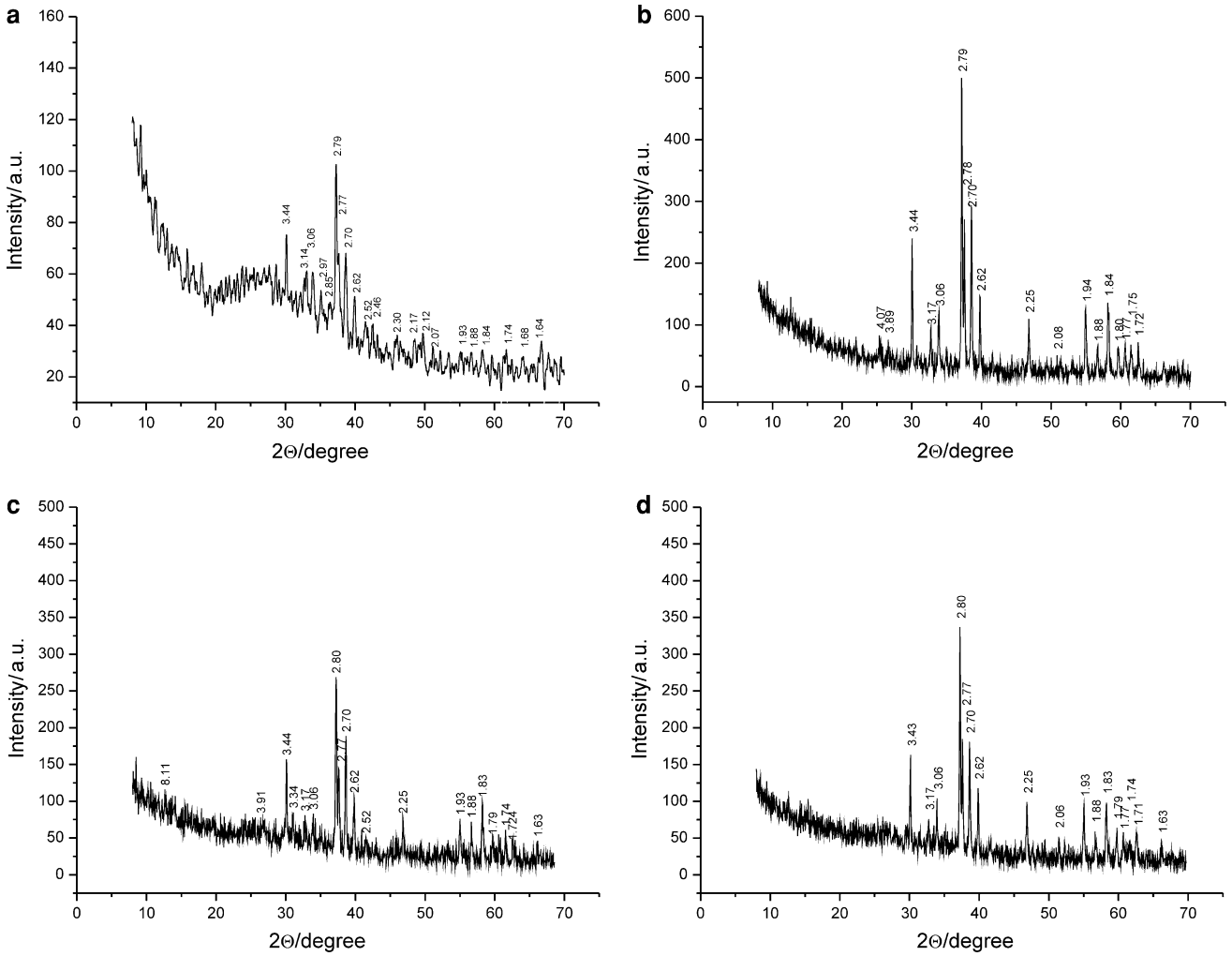

Fig. 1 Powder XRD patterns of the solid products from the thermal decomposition of Syrian phosphorite samples: **a** non-activated, **b** activated 30 min, **c** activated 150 min, **d** activated 300 min

Table 1 Results from the powder XRD phase analysis

Duration of MA (min)	Phases identified after the mechanical activation, PDF number/nm [12]	Phases identified after the mechanical activation and thermal treatment, PDF number/nm (this study)
0	$Ca_5F(PO_4)_3$ (15-0876) (FAp)—0.344; 0.279*; 0.2707; 0.262	$Ca_5F(PO_4)_3$ (15-0876)—0.279*; 0.270; 0.262
(sample A)	α quartz (46-0145)—0.334*, 0.425, 0.182	β-$Ca_3(PO_4)_2$ (03-0713)—0.285*, 0.317; 0.258
	$CaCO_3$ (47-1743)—3.03*, 0.193, 0.187	γ-Ca_2SiO_4 (24-0034)—0.274*; 0.304; 0.277, 0.248
		$CaSiO_3$ (42-0550)—0.297*; 0.309; 0.331
30	$Ca_5F(PO_4)_3$ (15-0876) (FAp)—0.344; 0.279*; 0.2707; 0.262	$Ca_5F(PO_4)_3$ (15-0876)—0.279*; 0.270; 0.262
(sample B)	α quartz (46-0145)—0.334*, 0.425, 0.182	$Ca_3(PO_4)_2 \cdot Ca_2SiO_4$ (73-1181)—0.282*; 0.261; 0.329
	$CaCO_3$ (47-1743)—3.03*, 0.193, 0.187	$Ca_4P_2O_9$ (11-0232)—0.280*; 0.277; 0.270
		$CaSiO_3$ (42-0550)—0.297*; 0.309; 0.331
150	$Ca_5F(PO_4)_3$ (15-0876) (FAp)—0.344; 0.279*; 0.2707; 0.262;	$Ca_5F(PO_4)_3$ (15-0876)—0.279*; 0.270; 0.262
(sample C)	α quartz (46-0145)—0.334*, 0.425, 0.182	
	$CaCO_3$ (47-1743)—3.03*, 0.193, 0.187	SiO_2 (46-0145)—0.334*; 0.426; 0.181
	$Ca_5(PO_4)_3OH$ (09-0432) (OHAp)—0.281*, 0.277, 0.270	γ-Ca_2SiO_4 (24-0034)—0.274*; 0.304; 0.277, 0.248
	$Ca_{10}(PO_4)_6CO_3$ (35-0180) (CAp)—0.283*, 0.277, 0.274	$CaSiO_3$ (42-0550)—0.297*; 0.309; 0.331
		$Ca_3(PO_4)_2 \cdot Ca_2SiO_4$ (73-1181)—0.282*; 0.261; 0.329
		$Ca_4P_2O_9$ (11-0232)—0.280*; 0.277; 0.270
300	$Ca_5F(PO_4)_3$ (15-0876) (FAp)– 0.344; 0.279*; 0.2707; 0.262;	$Ca_5F(PO_4)_3$ (15-0876)—0.279*; 0.270; 0.262
(sample D)	α quartz (46-0145)—0.334*, 0.425, 0.182	γ-Ca_2SiO_4 (24-0034)—0.274*; 0.304; 0.277, 0.248
	$CaCO_3$ (47-1743)—3.03*, 0.193, 0.187	$CaSiO_3$ (42-0550)—0.297*; 0.309; 0.331
	$Ca_5(PO_4)_3OH$ (09-0432)—0.281*, 0.277, 0.270	$Ca_3(PO_4)_2 \cdot Ca_2SiO_4$ (73-1181)—0.282*; 0.261; 0.329
	$Ca_{10}(PO_4)_6CO_3$ (35-0180)—0.283*, 0.277, 0.274	$Ca_4P_2O_9$ (11-0232)—0.280*; 0.277; 0.270

*strongest line

temperature reactions as a result of which γ-Ca_2SiO_4 and $CaSiO_3$ are obtained. Calcium silicophosphates are logically not detected at non-activated apatite as they are obtainable at considerably higher temperatures.

All products of the thermal synthesis are solid phases with close or overlapping diffraction lines which hinder their identification. As also reported by other authors [4], the obtained solid phase products represent solid solution of β-C_3P, γ -C_2Si, CSi, TTCP and FAp.

IR spectroscopy

IR spectra of the solid products from the thermal decomposition of the activated nanosized samples are presented in Fig. 2a–d and in Table 2.

The IR spectral analyses of nanosized activated samples of Syrian phosphorite examined in details in our previous publication have evidenced the bands of PO_4^{3-}, PO_3^{2-}, SiO_2, CO_3^{2-}, OH^- referring to the quartz, calcite, and apatite. Beside the stretching bands of the main phases ions there are also such ones that evidence the solid phase synthesis of β-$Ca(PO_3)_2$ and the isomorphous transformations of FAp, type B into COHFAp. COHFAp is of mixed A2-B type and can be presented by the generalized formula $Ca_{10-x}(PO_4)_{6-x}(F)_x(OH)_{2-x-2y}(CO_3)_y$, with $0 \leq x \leq 1.1$ and $0 \leq y \leq 0.2$ and deficiency regarding the calcium ions (calcium-deficient—Ca-def) [32, 33].

The IR spectra analysis of the same samples after heating up to 1,350 K (samples A-D) specifies that the registered absorption bands are related to the stretching modes of PO_4^{3-}, $PO_3^{2-}/P_2O_7^{4-}$, SiO_4^{4-}, SiO_3^{2-}, OH^-, and CO_2 caught from the air.

Most difficult for identification are the spectra of stretching and bending modes of the PO_4^{3-} group, although their presence is indisputable. The problem is in the overlapping and displacement of the bands of the separate phosphorous-containing phases. The bands at 570–580, 605–620 и 1,085 cm^{-1} (Fig. 2; Table 2) are results of the vibrations of the phosphate ion in FAp и β-C_3P. A tendency for displacement of the band at 605–630 cm^{-1} towards lower frequencies is registered. The spectra in Fig. 2 register the presence of new bands in the regions 475–490, 930–935, 950–965 and 1,225–1,250 cm^{-1}. They appear as a result of the formation of new phases in the process of the thermal decomposition of the mechanoactivated samples. Based on the performed analysis it is assumed that these bands characterize the vibrations of the POP (ν_3), PO_2 (ν_1) and PO_2 (ν_3) in di-($P_2O_7^{4-}$), tri-(PO_4^{3-}), tetra-($P_2O_9^{3-}$), and poly-(PO_3^{2-}) phosphates [24]. Due to overlapping of various vibrations

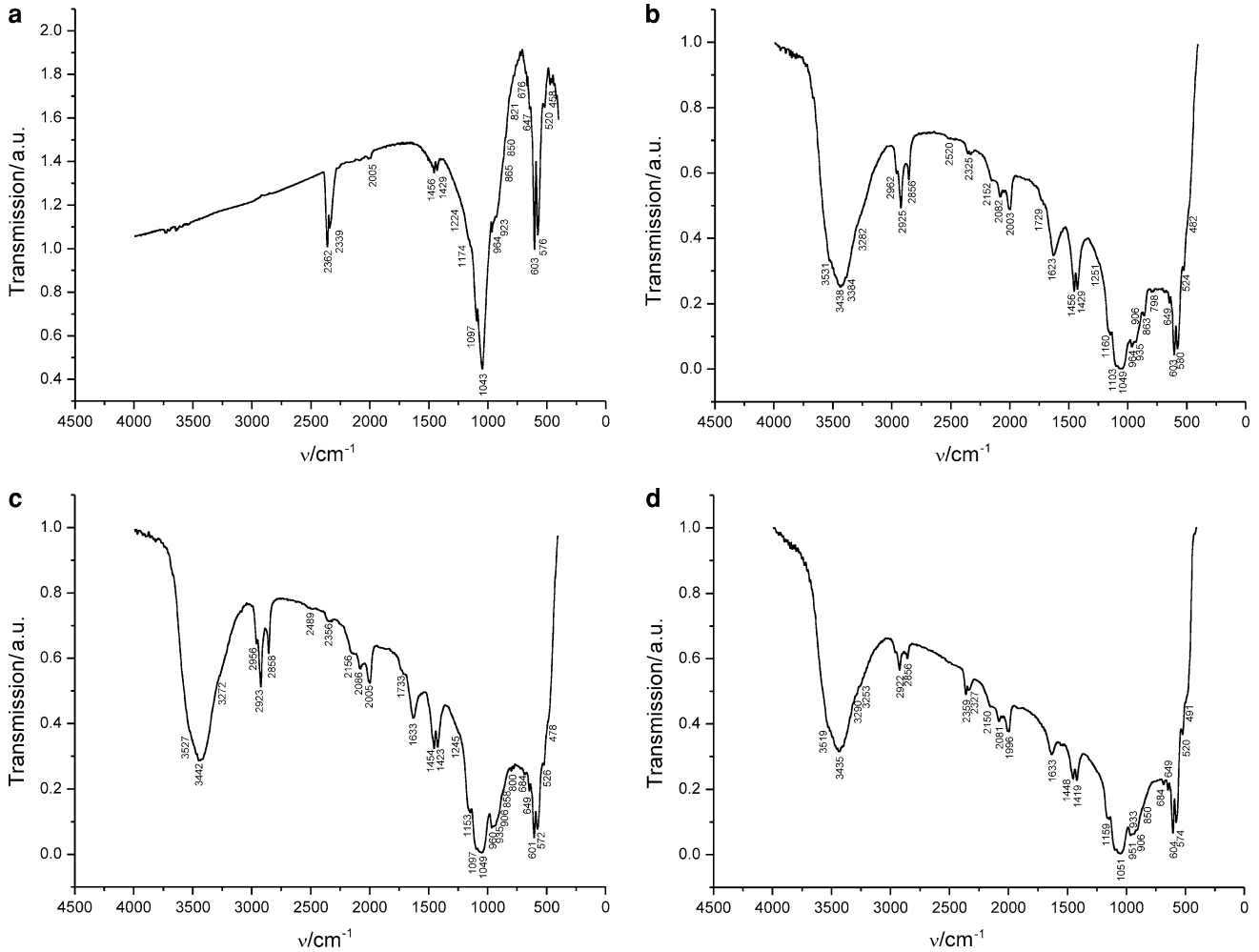

Fig. 2 IR spectra of the solid products from the thermal decomposition of Syrian phosphorite samples: **a** non-activated, **b** activated 30 min, **c** activated 150 min, **d** activated 300 min

of the phosphorous-containing ions, the compounds have been identified by some of the stand-alone and characteristic bands in their spectra. Thus, the bands at 570–605 and 1,085 cm^{-1} characterize PO_4^{3-} in FAp and β-C_3P (samples A-D) and the bands at 475–490 cm^{-1} and 1,225–1,250 cm^{-1}, evidence the presence of TTCP (samples B-D). TTCP is obtained upon the thermal decomposition of OHAp at temperatures above 1,550 K [12, 16]. Its identification among the solid products from the decomposition of nanosized activated samples of Syrian phosphorite at temperatures below 1,200 K [12] evidences again the increased reactivity of the activated nano-samples coming as result of the defectiveness and the set in substantial structural changes during the mechanochemical activation. Besides, the obtaining of TTCP is evidence for the formation of COHFAp in the course of the MA and leads to increase of the citric solubility.

These results are confirmed by the powder XRD analysis (Fig. 1; Table 1). In the powder XRD patterns (Fig. 1a–d) β-C_3P is identified as a separate phase only in the solid product after the heating of the non-activated Syrian phosphorite.

Due to the band overlapping of the di- and polyphosphate ions it is difficult to detect unambiguously their presence in the solid products after the thermal heating. These phases are not identified also by the powder XRD phase analysis.

The IR spectra of the thermally treated samples reveal intensity changes of the lines connected with the Si–O vibrations thus detecting the presence of α-SiO_2. These changes are related to the strong lowering of the intensity doublet at 775–793 cm^{-1} in the spectrum of the non-activated Syrian phosphorite, the overlapping of the two lines in nanosized samples B–C, and to the lack of such line in the spectrum of sample D (probably due to depletion of the amount of α-SiO_2) (Fig. 2a–d; Table 2). The established changes give ground to assume that during the thermal decomposition of samples A-D the α-SiO_2 transforms into

Table 2 Band positions and types of fundamental vibrations of samples of non-activated nanosized apatite after heat treatment at 1,350 K

No	Band position (cm^{-1})				Vibration mode
	0 min sample A	30 min sample B	150 min sample C	300 min sample D	
1.	458	–	–	–	Symmetric bending O–P–O (v_2) mode in β-C_3P [22]
2.	–	482	478	491	Symmetric O–P–O (v_2) bending mode in TTCP [23]
3.	520	524	526	520	Asymmetric O–Si–O (v_4) bending mode in γ-C_2Si [24, 25]
4.	576	580	572	574	Asymmetric O–P–O (v_4) bending mode in FAp [26]
	603	603	601	604	
5.	647	649	649	649	Asymmetric O–Si–O (v_4) bending mode in CSi [30]
	676	685	684	684	
6.	775	781	778	–	Symmetric Si–O (v_1) stretching mode in α–Si_2 [24]
	793				
7.	–	801	800	799	Symmetric Si–O–P (v_1) stretching mode in CSiP [29]
8.	850	–	–	850	Symmetric Si–O (v_1) stretching mode in γ-C_2Si [24, 25]
	865	863	858	–	
9.	–	906	906	906	Asymmetric Si–O (v_3) stretching mode in γ-C_2Si and CSi [24, 25, 30]
10.	923	935	935	933	Symmetric P–O (v_1) stretching mode in β-C_3P and TTCP [22]
	964	964	960	951	
11.	1,043	1,049	1,049	1,051	Asymmetric P–O (v_3) stretching mode in TTCP [23, 24]
	1,097	1,103	1,097	1,097	
12.	1,166	1,166	1,161	1,164	Symmetric P–O (v_1) stretching mode in $Ca(PO_3)_2$ and/or β-$Ca_2P_2O_7$ [24]
13.	1,224	1,251	1,245	1,251	Asymmetric P–O (v_3) stretching mode in TTCP and/or $Ca(PO_3)_2$ [23, 24]
14.	1,429	1,429	1,423	1,419	Symmetric OH^- (v_2) bending mode Si–O–Si–OH and/or Si–O–P–OH between oxygen-silicon (SiO_4^{4-}) and/or oxygen–phosphate (PO_3^{4-}) tetrahedrons [23, 29]
	1,456	1,454	1,454	1,448	
15.	–	1623	1,633	1,633	Symmetric OH^- (v_2) bending mode in crystal water [27]
	–	1,729	1,733	–	
16.	2,005	2,003	2,005	1,996	Asymmetric (v_3) stretching mode of P–O in PO_4^{3-} [31]
		2,082	2,086	2,081	
		2,152	2,156	2,150	
17.	2,339	2,325	–	2,327	Asymmetric C–O (v_3) stretching mode in CO_2 (air) [25]
	2,369	–	2,356	2,359	
18.	–	2,800–3,500	2,800–3,500	2,800–3,500	Asymmetric O–H (v_1) stretch H_2O [27, 31]
19.	–	3,531	3,527	3,519	Asymmetric O–H (v_1) stretch OH^- [31]

structures of higher symmetry. The appearance of new bands at 520, 850–865, 906 cm^{-1} is also good evidence for the accuracy of such assumption. They are attributed to the bending and stretching modes of the SiO_4^{4-} and SiO_3^{2-} tetrahedra in the γ-larnite (γ-Ca_2SiO_4—520, 850–865, 906 [24, 25]) and wollastonite ($CaSiO_3$—647–685, 906 [30]). Most probably, α-quartz takes part in the solid state reactions of formation of CSiP and/or γ-C_2Si, CSi and some minor amounts remain in the solid state products being on the boundary of the spectral resolution. Therefore, it can be assumed that there are traces of α-quartz in the solid products after heating of samples A-D which does not affect the results of the carried out investigation.

According to Stoch [28] a symmetric stretching of the bond Si–O–P is detected at 800 cm^{-1}, which evidence the formation of a valence bridge between the SiO_4^{4-} and PO_4^{3} tetrahedra. The existence of such bridge is attributed to the presence of calcium silicophosphate $Ca_3(PO_4)_2 \cdot Ca_2SiO_4$ (CSiP). The absorption bands of SiO_4^{4-} and PO_4^{3-} and the valence bridge between the two type tetrahedra give reason to assume that after heating to 1350 K CSiP is formed in the solid products.

The IR spectra give also evidence for the presence of OH^- groups connected by loose hydrogen bonds at 1,620–1,740 cm^{-1} (Fig. 2; Table 2), which specifies that H_2O is present both as adsorbed on the active surface and as water of crystallization. This can be expected considering the heating of the activated samples which consequently easily adsorb atmospheric water. The absorption bands in the range 1,420–1,460 cm^{-1} in the spectra of heated samples can be interpreted as being due to the presence of a carbonate-containing component. This is less likely having in mind the high end temperature of heating (1,350 K), as well as the lack of the characteristic band of symmetric bending mode of O–C–O (ν_2) for the CO_3^{2-} group at 870 cm^{-1}. It can be assumed that the appearance of absorption bands in this range is related to the bending modes of the OH^- groups placed on the vertices of the silicon tetrahedra, regardless of the degree of their occupancy [22].

The functional groups that give evidence for the presence of FAp, β-C_3P, TTCP, CSiP, C_2Si, CSi, $Ca(PO_3)_2$ and/or γ-$Ca_2P_2O_7$ in the solid phase products after the thermal decomposition to 1,350 K of nanosized samples of Syrian phosphorite are determined based on known reference data and the carried out analysis, the results of which are presented in Table 2 and Fig. 2a–d. The main phases in sample A are FAp, β-C_3P, γ-C_2Si, CSi as separate phases and in the mechanoactivated samples (B-D) main phase is FAp and as a result of the thermal reaction—CsiP (most probably in the form of crystalline hydrate), TTCP, γ-C_2Si, CSi, $Ca(PO_3)_2$ and/or γ-$Ca_2P_2O_7$. These results are also supported by the powder XRD data.

The obtained spectroscopic results can be supported by data of the thermal investigations carried out with non-activated and activated samples of Syrian phosphorite which is the main objective of the present work.

DTA-DTG-TG analyses

The results of the carried out thermal analysis of inctivated and activated in planetary mill for 30 to 300 min nanosized samples of Syrian phosphorite are presented in Fig. 3 and Table 3.

Total mass losses of 7.8% are detected in the course of the thermal treatment of non-activated Syrian phosphorite

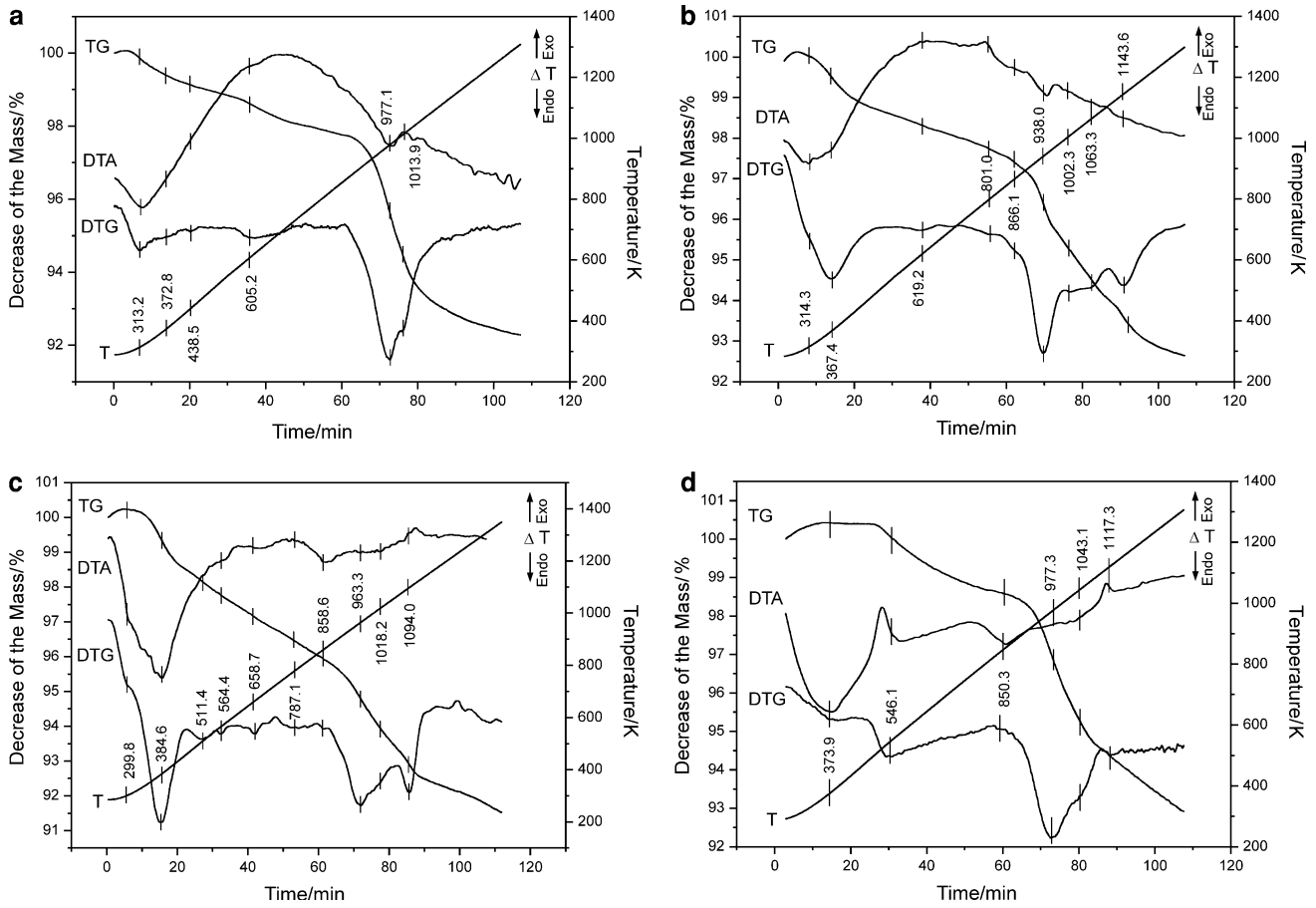

Fig. 3 TG-TDA-DTG of Syrian phosphorite samples: **a** non-activated, **b** activated 30 min, **c** activated 150 min, **d** activated 300 min

Table 3 Dynamics of the mass losses upon thermal treatment of Syrian phosphorite up to 1,350 K depending on the mechanochemical duration

Stage	Activation durability (min)							
	Initial phosphorite (sample A)		30 (sample B)		150 (sample C)		300 (sample D)	
	T/K	Mass losses (%)	T/K	Mass losses (%)	T/K	Mass losses (%)	T/K	Mass losses (%)
1	291.9–350.3	0.6	296.6–324.7	0.2	290.7–315.7	0.1	–	–
2	350.3–418.0	0.3	324.7–486.8	1.2	315.7–452.9	1.6	325.9–509.6	0.1
3	418.0–476.1	0.2	–	–	–	–	–	–
4	–	–	–	–	452.9–546.2	0.6	–	–
5	–	–	–	–	546.2–613.1	0.4	509.6–777.4	1.4
6	557.6–733.4	0.8	566.6–669.1	0.3	613.1–713.3	0.7	–	–
7	–	–	759.4–834.5	0.2	713.3–832.0	0.7	–	–
8	–	–	834.5–891.8	0.4	832.0–880.0	0.3	762.7–891.1	0.4
9	860.4–1,002.3	2.8	891.8–978.9	1.6	880.0–986.2	1.4	891.1–1023.4	2.7
10	1,002.3–1,101.3	1.7	978.9–1,038.8	0.8	986.2–1,069.0	1.1	–	–
11	–	–	1038.8–1,104.2	0.8	1,069.0–1,106.1	0.5	1,023.4–1,097.3	1.1
12	–	–	1,104.2–1,204.2 endo	1.0	1,106.1–1,144.8 exo	0.4	1,097.3–1,153.0 exo	0.5
Total		7.8		7.5		8.8		7.4

to 1,350 K (Fig. 3a; Table 3). They can be attributed to the release of physisorption water and water of crystallization, liberation of structurally bound CO_2 and decarboxylation of separately existing carbonates. The physisorption water and the water of crystallization are liberated within a wide temperature range between 373–783 K, while the dehydroxylation and the liberation of CO_2 either incorporated in the apatite structure or being on the account of separately existing carbonates occur above 893 K. The endothermic effect registered in the temperature area 842–981 K is attributed to the liberation of CO_2, located in the tetrahedral positions of the phosphate ion in the apatite structure, a fact that supports the spectroscopic results according to which the initial Syrian phosphorite is specified as carbonate fluorine apatite (CFAp) type B [12].

$$\begin{aligned} Ca_{10}(PO_4)_6F_{2-2x}(CO_3)_x = {} & Ca_5(PO_4)_3F \\ & + Ca_3(PO_4)_3 + (1+x)/2CaO \\ & + Ca_{(1-x)/2}F_{1-x} + xCO_2 \\ & + x/2O_2 \end{aligned} \quad (1)$$

where $0 \leq x \leq 1.0$ [32]

The obtained whitlockite is the more low-temperature and X-ray amorphous β-modification [34].

The endothermic effect registered in the temperature range 980–1,050 K is result of decarboxylation of the mineral calcite available in the initial phosphorite.

$$CaCO_3 = CaO + CO_2 \quad (2)$$

Based also on the spectroscopic investigation it can be assumed that in the high temperature ranges a solid phase interaction between CFAp and quartz takes place resulting in the formation of C_3P and C_2Si according to the following reaction:

$$\begin{aligned} 2Ca_5F(PO_4)_3 + SiO_2 + 2CaO = {} & 3Ca_3(PO_4)_2 + Ca_2SiO_4 \\ & + CaF_2 \end{aligned} \quad (3)$$

as well as

$$CaO + SiO_2 = CaSiO_3 \quad (4)$$

The data presented give evidence that the apatite which is major component in the natural phosphates is thermally stable within the studied temperature range

The results of the thermal analysis performed on nanosized activated samples of Syrian phosphorite (Fig. 3b–d; Table 3) differ from those ones of the non-activated sample (Fig. 3a; Table 3). New effects are registered in the thermograms in Fig. 3 in the ranges up to 600 K and in the following temperature ranges 770–800, 850–870, 1,040–1,100 and 1,120–1,130 K, accompanied by increase of the mass losses. The obtained data are analyzed considering as the presence of the new phases formed during the activation process as well as the overlapping of the effects from various thermal reactions which makes their interpretation difficult.

In the low-temperature area up to 600 K the endothermic effects in the thermograms of the activated nanosized samples of Syrian phosphorite are attributed to the dehydration of the obtained crystalline hydrates which are hard for identification by means of the used spectroscopic methods due to the predominant content of CFAp. The

formation of the non-stoichiometric crystalline hydrates comes as a result of the exposure of new surfaces during the mechanochemical activation which subsequently interact with the atmospheric components and mainly with the aqueous vapor.

Low-intensity endothermic effects accompanied by 0.4–0.7% mass loss are registered in the region 460–620 K (Table 3). They are best expressed in sample C. As also mentioned by Ivanova [4, 33] these effects can be explained with the relocation of CO_2^{3-} in the interchannel space close to the hexagonal axis in which part of the carbonate ions separate in gaseous phase and mass loss of approximately 0.4% is registered.

The endothermic effects in the temperature range 620–700 K (best expressed in sample C, 660 K), can be explained with the proceeding of a thermal reaction between $CaH_2P_2O_7$ and $CaCO_3$ (reaction 5), data for which have also been reported by other authors [5]:

$$CaH_2P_2O_7 + 2CaCO_3 = Ca_3(PO_4)_2 + 2CO_2 + H_2O \quad (5)$$

The identification of $CaH_2P_2O_7$ in samples containing SiO_2 is very difficult. The strongest diffraction line in the pattern of $CaH_2P_2O_7$ is at $d = 0.334$ nm (51-0200). It coincides with the strongest line of SiO_2 (46-1045), which dominates in the patterns of the activated nano-sized samples [12]. The other lines at $d = 0.376$ nm and $d = 0.318$ nm are very weakly presented due to the strong lowering of the lines intensity in the XRD patterns of samples B-D as a result of the carried out mechanochemical activation. The IR spectroscopy data are also ambiguous [12] regarding the presence of the $P_2O_7^{4-}$ group. That is why the hydro-pyrophosphate was not identified in our previous work [12]. This becomes possible upon thermal decomposition of the activated samples and detection of the thermal effects in the range 620–700 K, which are missing for the non-activated Syrian phosphorite.

The registered weak endothermic effect in the temperature range 770–800 K related to 0.7–0.8% mass losses in samples B and C is missing on the DTA curves of samples A and D. These losses can be explained with the decomposition of $Ca(OH)_2$ obtained as a by-product when atmospheric water is adsorbed after the samples activation. The lack of this effect in sample A is reasonable. As for the case of sample D it is assumed to be due to the longer activation time. The lack of mass losses at lower temperatures is probably due to the same phenomenon. The established changes in the thermogram of sample D (Fig. 3d) correspond to the results of electron microscopy establishing the formation of plastic flow causing intensive agglomeration of the nanosized particles [12]. The latter leads to decrease in the rate of the mechanochemical processes in cases when activation duration varies from 150 to 300 min and increase of the temperature ranges of conversion.

A new endothermic effect is registered in the temperature range from 850 to 870 K in samples B-D. Its appearance is explained by the liberation of CO_3^{2-} ions substituting F^- along the apatite hexagonal axis. As already reported, [1, 10, 15, 16, 34–40] the liberation of CO_3^{2-} ions from the A2 positions precedes the same process from the B positions and the structurally non-involved carbonates decompose at highest temperatures. This demonstrates the structural changes taking place during the mechanochemical activation and respectively the CO_3^{2-} migration from the PO_4^{3-} positions and/or the incorporation of CO_2 in the substitution scheme of the univalent ion. The presence of separately existing calcite also contributes to the incorporation of CO_3^{2-} ions in the hexagonal positions and the conversion of COHFAp type B into type A2 [1, 15]. This result supports the IR spectroscopic data about the formation of COHFAp type A2 (Ca-def) [12, 15, 35] during activation of the nanosized samples B-D (Fig. 2b–d; Table 2).

Highest mass losses for all samples, values of 1.4–2.8%, can be registered within the temperature range 930–980 K and they are due to the liberation of CO_3^{2-} incorporated in the positions of the phosphate ion. Namely these thermal effects characterize the non-activated Syrian phosphorite (sample A) as CFAp type B and the activated samples (B-D) as apatite of mixed type substitution (A2 and B) regarding the CO_3^{2-} group [1, 10, 15]. The formation of OHFAp is most probably due to the decompositions taking place up to these temperatures.

Thermal reactions between the β-$Ca(PO_3)_2$ obtained during the mechanochemical activation and $CaO/CaCO_3$ are possible in the same temperature area as follows:

$$Ca(PO_3)_2 + CaO = Ca_2P_2O_7 \quad (6)$$

and/or

$$Ca(PO_3)_2 + CaCO_3 = Ca_2P_2O_7 + CO_2 \quad (7)$$

The presence of calcium pyrophosphate in the solid phase products after the heating (Table 2) can be explained through these reactions which due to overlapping of the diffraction lines in the powder XRD patterns (Fig. 1; Table 1) and that one of the bands in the IR spectra (Fig. 2; Table 2) can hardly be identified.

The decomposition of the separately existing carbonate, supposed to be calcite or aragonite is registered in the next temperature range—980–1,020 K. It is referenced that during the mechanochemical activation $CaCO_3$ from the non-activated phosphorite undergoes phase transition to aragonite [1]. Its identification is hard due to the nanosized nature of the samples obtained. The registered mass losses within the pointed temperature range decrease from 1.7% in

sample A to 1.0% in sample C which can be explained with the possible participation of $CaCO_3$ in the thermal reactions and with the phase deformations taking place during the activation already in the lower temperature ranges. With increase of the time for mechanochemical activation, general lowering of the temperatures and overlapping of the endothermic effects caused by the carbonate ions decomposition from the three type positions is observed and namely: CO_3^{2-} substituting the univalent fluorine ion (position A2); CO_3^{2-}, substituting the phosphate ion (position B) and the separately existing carbonate (Fig. 3d).

The endothermic effects occurring in the temperature range 1,040–1,100 K are new for samples B-D and missing for the non-activated Syrian phosphorite. Therefore, their appearance can be considered as a direct result of the mechanochemical activation. The proceeding interactions can be described by reactions of decomposition of the formed in the period of the heating OHFAp to C_3P and TTCP, identified also by the physical methods (Table 1; Fig. 1; Table 2, and Fig. 2), following reaction (8):

$$Ca_{10}FOH(PO_4)_6 = 2Ca_3(PO_4)_2 + Ca_4P_2O_9 + HF \quad (8)$$

This thermal reaction is best expressed in sample C (Fig. 3c).

The formation of the spectroscopically detected CSiP in the high temperature area (1,100–1,220 K) [41, 42] is interpreted as a result of an interaction between C_3P, α-SiO_2 and the free CaO following reaction 9:

$$Ca_3(PO_4)_2 + 2CaO + SiO_2 = Ca_3(PO_4)_2Ca_2SiO_4 \quad (9)$$

The solid phase synthesis reaction runs without mass losses, however, an exothermic peak near 1,115–1,117 K is registered being due as well to the relaxation of the accumulated mechanical energy (samples C and D, Fig. 3c–d; Table 3). Its release facilitates the relaxation of the metastable solid phase into energetically more stable equilibrium state with run products described in Table 1 and Table 2. Theoretically, the CaSiP synthesis should take place at higher temperatures. However, the impact of the mechanochemical activation on the formation of highly active nanosized and energetically loaded phase makes possible the considerable lowering of the synthesis temperature. Despite the overlapping of the diffraction lines in the powder XRD patterns and that one of the adsorption bands in the IR spectra the obtained results give good ground to assume the formation of $Ca_3(PO_4)_2 \cdot Ca_2SiO_4$ as a result of solid phase synthesis under the specific experimental conditions.

The TG-DTA-DTG data complement and further clarify the results obtained in our previous work [12]. The appearance of additional thermal effects in the temperature range 850–870 K is unambiguously interpreted as being due to the isomorphous substitutions and placement of CO_3^{2-} ions in crystallographically non-equivalent positions in the apatite structures of samples B-D. The type of the initial Syrian phosphorite as being CFAp type B has also been confirmed.

Conclusions

The following conclusions can be drawn from the obtained thermal, spectroscopic and powder XRD investigations of the studied decomposition solid products:

1. The thermal analysis of non-activated and mechanochemically activated nanosized samples of Syrian phosphorite further clarify and advance our previously reported conclusions concerning the studied structural transformations. The formation of COHFAp type A2-B is unambiguously confirmed by the thermal effects evidencing reactions of decomposition of isomorphously substituted carbonate and hydroxyl ions in the vicinity of the 6_3 axis as well as that one of the carbonate ions substituting the phosphate ions.
2. Product of the mechanochemical activation is a nanosized highly active and energetically loaded phase which relaxes upon temperature elevation through decomposition of the contained hydroxyl and carbonate ions as well as through solid phase transformations yielding β-C_3P, TTCP, β-C_2Si and CSiP as run products.
3. The α-SiO_2 and calcite participation in the phase transformations and isomorphous conversions evidence the impact of the mechanochemical activation over the concomitant minerals in the initial phosphorite. Their presence facilitates the apatite structure destabilization and the subsequent appearance in the nanosized samples of properties.

It is difficult to give synonymous answer about the best activation conditions at this stage of the investigations. Main advantage of the samples treated for 30 min is their high reactivity and active surface. The samples treated up to 300 min are characterized by highest defectiveness of the structure and mechanical energy accumulation. Its relaxation can be used to increase the effectiveness of the mechanochemical activation.

Acknowledgements The authors thank the National Fund "Scientific research" of the Ministry of Education for the financial support (project DOO2-104).

References

1. Chaikina MV. Mechanochemistry of natural and synthetic apatites. In: Avvakumov EG, editor. Novosibirsk: Publishing house of SB RAS, Branch "GEO"; 2002. p. 11–15; 105–107; 114–115; 139.

2. Pelovski Y, Petkova V, Dombalov I. Thermotribochemical treatment of low grade natural phosphates. J Therm Anal Calorim. 2007;88:207–12.
3. Wieczorek-Ciurowa Kr, Gamrat K. Mechanochemical syntheses as an example of green processes. J Therm Anal Calorim. 2007; 88:213–7.
4. Tonsuaadu K, Rimm K, Veiderma M. Composition and properties of thermophosphates from apatite and aluminosilicates. Phosphorus Sulphur Silicon. 1993;84:73–81.
5. Tonsuaadu K, Peld M, Leskela T, Mannonen R, Niinisto L, Veiderma M. A thermoanalytical study of synthetic carbonate-containing apatites. Thermochim Acta. 1995;256:55–65.
6. Veiderma M, Knubovets R, Tonsuaadu K. Fluorhydroxyapatites of Northern Europe and their thermal transformations. Phosphorus Sulphur Silicon. 1996;109–110:43–6.
7. Kaljuvee T, Kuusik R, Veiderma M. Physico-chemical transformations during thermal treatment of phosphorites and solubility of the products. Phosphorus Res Bull. 1999;10:335–40.
8. Chatzistavrou X, Zorba T, Chrissafis K, Kaimakamis G, Kontonasaki E, Koidis P, et al. Influence of particle size on the crystallization process and the bioactive behavior of a bioactive glass system. J Therm Anal Calorim. 2006;85:253–9.
9. da Silva Filho EC, da Silva OG, da Fonseca MG, Arakaki LNH, Airoldi C. Synthesis and thermal characterization of copper and calcium mixed phosphates. J Therm Anal Calorim. 2007;87:775–8.
10. Lafon JP, Champion E, Bernache-Assollant D, Gibert R, Danna AM. Thermal decomposition of carbonated calcium phosphate apatites. J Therm Anal Calorim. 2003;73:1127–34.
11. Bianco Al, Cacciotti I, Lombardi M, Montanaro L, Gusmano G. Thermal stability and sintering behaviour of hydroxyapatite nanopowders. J Therm Anal Calorim. 2007;88:237–43.
12. Yaneva V, Petrov O, Petkova V. Structural and spectroscopic studies of the nanosize appatite (Syrian). Mater Res Bull. 2009; 44:693–9.
13. Nikcevic I, Jokanovic V, Mitric M, Nedic Z, Makovec D, Uskokovic D. Mechanochemical synthesis of nanostructured fluorapatite/fluorhydroxyapatite and carbonated fluorapatite/fluorhydroxyapatite. J Solid State Chem. 2004;177:2565–74.
14. McCubbin FM, Mason HE, Park H, Phillips BL, Parise JB, Nekvasilil H, et al. Synthesis and characterization of low-OH–fluor-chlorapatite: a single-crystal XRD and NMR spectroscopic study. Am Mineral. 2008;93:210–6.
15. Chrisis Tacker R. Carbonate in igneous and metamorphic fluorapatite: two type A and two type B substitutions. Am Mineral. 2008;93:168–76.
16. Lafon JP, Championa E, Bernache-Assollant D. Processing of AB-type carbonated hydroxyapatite $Ca_{10-x}(PO_4)_{6-x}(CO_3)_x(OH)_{2-x-2y}(CO_3)_y$ ceramics with controlled composition . J Eur Ceram Soc. 2008;28:139–47.
17. Suetsugu Y, Takahashi Y, Okamura FP, Tanaka J. Structure analysis of A-type carbonate apatite by a single-crystal X-ray diffraction method. J Solid State Chem. 2000;155:292–7.
18. Fleet ME, Liu X. Carbonate apatite type A synthesized at high pressure: new space group (P3) and orientation of channel carbonate ion. J Solid State Chem. 2003;174:412–7.
19. LeGeros RZ, Trautz OR, Klein E, LeGeros JP. Two types of carbonate substitution in the apatite structure Experimentia. 1969;25:5–7.
20. Elliott JC. In: Kohn MJ, Rakovan J, Hughes JM, editors. Phosphates Rev Miner Geochem, vol. 48. Miner Soc Am, Washington, DC; 2002. p. 427.
21. Tõnsuaadu K, Peld M, Bender V. Thermal analysis of apatite structure. J Therm Anal Calorim. 2003;72:363–71.
22. Jillavenkatesa A, Condrate RA Sr. The infrared and Raman spectra of β-and α-tricalcium phosphate ($Ca_3(PO_4)_2$). Spectrosc Lett. 1998;31:1619–34.
23. Jillavenkatesa A, Condrate RA Sr. The infrared and Raman spectra of tetracalcium phosphate ($Ca_4P_2O_9$). Spectrosc Lett. 1997;30:1561–70.
24. Plusnina I. Infrared spectroscopy of the minerals. Moscow; 1977 (in Russian).
25. Nakamoto K. Infrared and Raman spectra of inorganic and coordination compounds. 4th ed. New York: Wiley; 1986.
26. Shi J, Klocke A, Zhang M, Bismayer U. Thermally-induced structural modification of dental enamel apatite: decomposition and transformation of carbonate groups. Eur J Miner. 2005;17: 769–75.
27. Uhnevish G. Infrared spectroscopy of the water (edited by prof. L.A. Gribov). Nauka, Moscow; 1973 (in Russian).
28. Stoch L, Środa M. Infrared spectroscopy in the investigation of oxide glasses structure. J Mol Struct. 1999;511/512:77–84.
29. Ciecinska M. Thermal analysis of gel-derived bioactive phosphosilicate glasses. J Therm Anal Calorim. 2003;72:199–207.
30. Ryall W, Threagold I. Evidence for $[(SiO_3)_5]\{\infty\}$ type chains in inesite as shown by X-ray and infrared absorption studies. Am Mineral. 1966;51:754–61.
31. Wilson RM, Elliott JC, Dowker SEP. Formate incorporation in the structure of Ca-deficient apatite: rietveld structure refinement. J Solid State Chem. 2003;174:132–40.
32. Meejoo S, Maneeprakorn W, Winotai P. Phase and thermal stability of nanocrystalline hydroxyapatite prepared via microwave heating. Thermochim Acta. 2006;447:115–20.
33. Barralet J, Knowles J, Best S, Bonfield W. Thermal decomposition of synthesised carbonate hydroxyapatite. J Mater Sci: Mat Med. 2002;13:529–33.
34. Ivanova TI, Frank-Kamenetskaya OV, Kol'tsov AB, Ugolkov VL. Crystal structure of calcium-deficient carbonated hydroxyapatite. Thermal decomposition. J Solid State Chem. 2001;160: 340–9.
35. He QJ, Huang ZL, Cheng XK, Yu J. Thermal stability of porous A-type carbonated hydroxyapatite spheres. Mater Lett. 2008;62: 539–42.
36. Shi Donglu, editor. Biomaterials and tissue engineering. Berlin, New York: Springer/Tsinghua University Press; 2004.
37. Elliott JC. Structure and chemistry of the apatites and other calcium orthophosphates. Amsterdam: Elsevier; 1994.
38. Trojan M, Šulcová P, Sýkorová L. Thermal analysis of Ba(II)–Sr(II) cyclo-tetraphosphates(V). J Therm Anal Calorim. 2002;68: 75–9.
39. Shi J, Klocke A, Zhang M, Bismayer U. Thermal behavior of dental enamel and geologic apatite: an infrared spectroscopic study. Am Mineral. 2003;88:1866–71.
40. Holcomb DW, Young RA. Thermal decomposition of human tooth enamel. Calcif Tissue Int. 1980;31:189–201.
41. Sitarz M, Szumera M. Crystallization of silico-phosphate glasses. J Therm Anal Calorim. 2008;91:255–60.
42. Szumera M, Wacławska Ir. Spectroscopic and thermal studies of silicate-phosphate glass. J Therm Anal Calorim. 2007;88:151–6.